ACS chemical biology

Letters

pubs.acs.org/acschemicalbiology

# HyPer-3: A Genetically Encoded $H_2O_2$ Probe with Improved Performance for Ratiometric and Fluorescence Lifetime Imaging

Dmitry S. Bilan,[†,‡] Luke Pase,[∥] Linda Joosen,[⊥] Andrey Yu. Gorokhovatsky,[‡,#] Yulia G. Ermakova,[‡,§] Theodorus W. J. Gadella,[⊥] Clemens Grabher,[∥] Carsten Schultz,[¶] Sergey Lukyanov,[†,‡] and Vsevolod V. Belousov*[,†,‡]

[†]Nizhny Novgorod State Medical Academy, Nizhny Novgorod, Russia

[‡]Shemyakin-Ovchinnikov Institute of Bioorganic Chemistry, 117997 Moscow, Russia

[§]Faculty of Biology, Moscow State University, Moscow, Russia

[∥]Karlsruhe Institute of Technology, Forschungszentrum Karlsruhe GmbH, Institute of Toxicology and Genetics, 76344 Eggenstein-Leopoldshafen, Germany

[⊥]Swammerdam Institute for Life Sciences & Netherlands Institute for Systems Biology, University of Amsterdam, NL-1098 XH Amsterdam, The Netherlands

[#]Shemyakin-Ovchinnikov Institute of Bioorganic Chemistry, Pushchino Branch, Pushchino, Russia

[¶]European Molecular Biology Laboratory, 69117 Heidelberg, Germany

**ABSTRACT:** High-performance sensors for reactive oxygen species are instrumental to monitor dynamic events in cells and organisms. Here, we present HyPer-3, a genetically encoded fluorescent indicator for intracellular $H_2O_2$ exhibiting improved performance with respect to response time and speed. HyPer-3 has an expanded dynamic range compared to HyPer and significantly faster oxidation/reduction dynamics compared to HyPer-2. We demonstrate this performance by *in vivo* imaging of tissue-scale $H_2O_2$ gradients in zebrafish larvae. Moreover, HyPer-3 was successfully employed for single-wavelength fluorescent lifetime imaging of $H_2O_2$ levels both *in vitro* and *in vivo*.

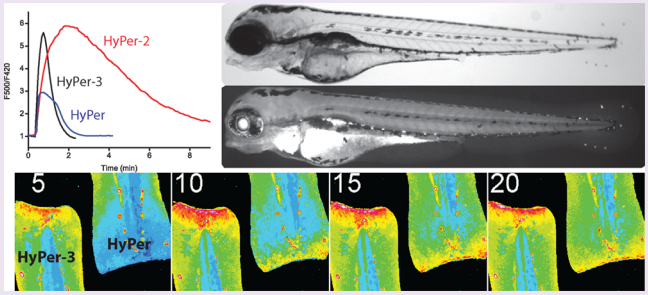


Reactive oxygen species (ROS) are products of incomplete molecular oxygen reduction. Among ROS, the superoxide anion radical $O_2^{*-}$ and hydrogen peroxide $H_2O_2$ are the most investigated in biology because they are produced by a wide range of enzymes, specifically or as side-products, and have a number of well-known biological effects.[1] For a long time, ROS were viewed mostly in a context of their nonspecific damaging action on DNA, lipids, and proteins.[2] This point of view was strongly supported by the discovery of antioxidant enzymes decomposing ROS and by the fact that phagocytes produce ROS when killing pathogens.[1,3] Later, the ROS toxicity dogma was challenged after specialized $O_2^{*-}$ and $H_2O_2$ producing enzymes were found to be expressed in most cell types.[4,5] This fact gave a new impulse to ROS investigations but, now in the context of their regulatory function, as signaling molecules. It was shown that $H_2O_2$ acted as a second messenger selectively oxidizing those cysteine residues in proteins that were ionized (deprotonated) at physiological pH values.[6,7] Initially, protein tyrosine phosphatases were shown to be reversibly inactivated by $H_2O_2$.[8,9] Since then, the list of known redox regulated proteins grew exponentially. During the last years, proteomics and computational approaches added a lot of new members to the list.[10,11]

Until recently, no probes existed allowing specific ROS detection within living cells. Within the last years, a number of methods appeared including a palette of $H_2O_2$ sensitive synthetic dyes[12] and two genetically encoded sensors,[13] HyPer[14] (later version, HyPer-2[15]) and roGFP2-Orp1.[16] HyPer consists of a circularly permuted yellow fluorescent protein (cpYFP) integrated into a regulatory domain of the $H_2O_2$ sensing protein OxyR.[14] Wild-type OxyR consists of two domains, a DNA-binding and a regulatory (OxyR-RD) domain.[17] OxyR-RD contains two cysteine residues, C199 and C208, which determine its $H_2O_2$ sensitivity.[18] C199 is inaccessible for charged oxidants such as superoxide because it is positioned in a hydrophobic pocket. However, $H_2O_2$ penetrates the pocket and oxidizes C199 to a charged sulphenic acid intermediate that is then repelled by its hydrophobic surround. Initially separated, C199 and C208 get sufficiently close to form a disulfide bridge. Upon disulfide formation, the conformation of the OxyR-RD drastically changes allowing

**Received:** September 10, 2012
**Accepted:** December 20, 2012
**Published:** December 20, 2012

   dx.doi.org/10.1021/cb300625g | *ACS Chem. Biol.* 2013, 8, 535–542

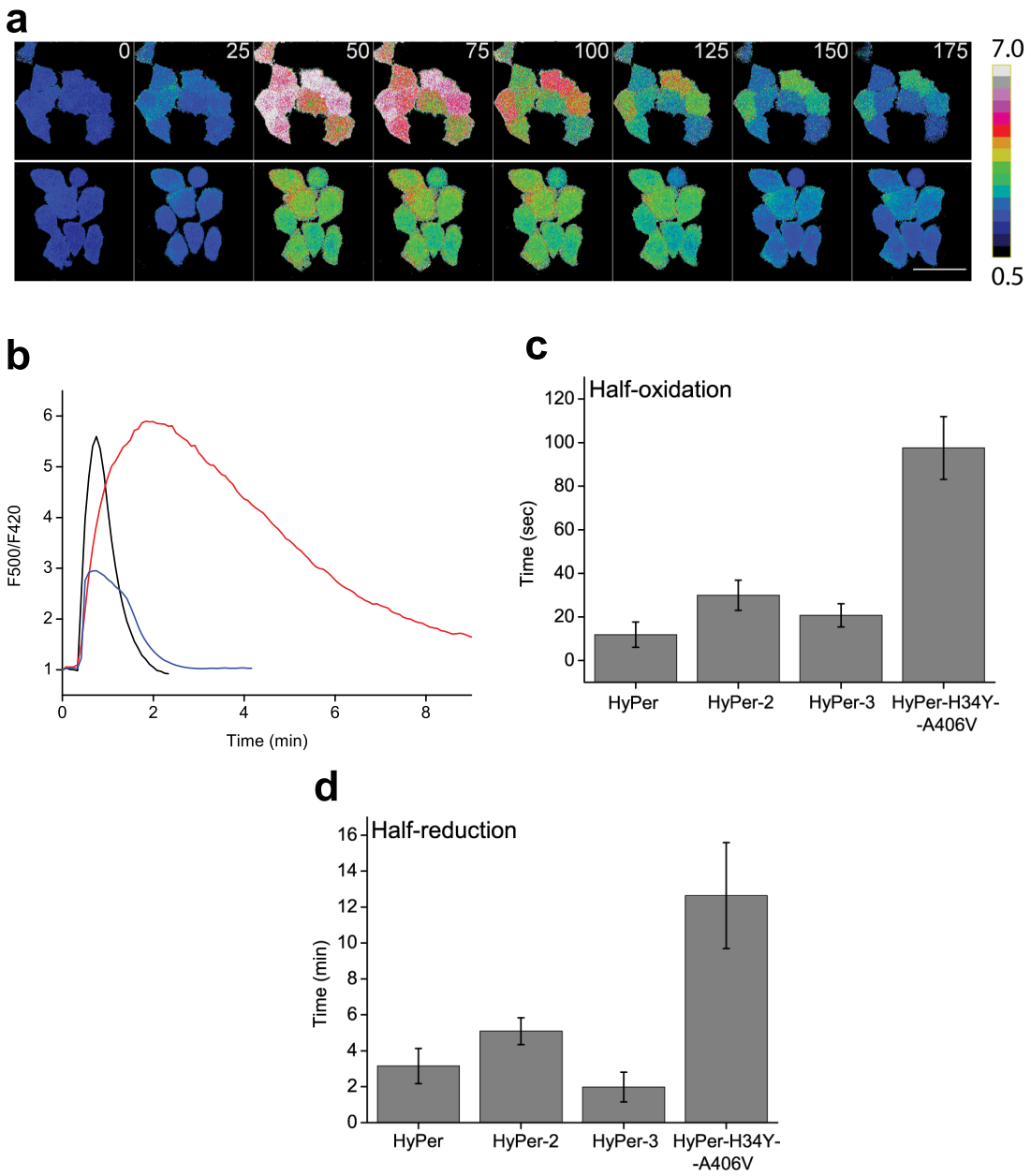


**Figure 1.** HyPer-3 vs HyPer and HyPer-2 response to $H_2O_2$. (a) Images of F500/F420 ratio in cells transiently transfected with HyPer-3 (upper row) or HyPer (lower row) exposed to 150 $\mu$M of $H_2O_2$. Numbers indicate timing in seconds. Scale bar, 40 $\mu$m. Lookup table indicates F500/F420 ratio. (b) Timing of $H_2O_2$ induced ratio change in individual cells expressing HyPer-3 (black line) compared to HyPer (blue line) and HyPer-2 (red line). (c) Half-oxidation times of HyPer, HyPer-2, HyPer-3, and HyPer-H34Y-A406V upon the addition of $H_2O_2$. Zero time corresponds to the moment of $H_2O_2$ addition. Error bars indicate standard deviation. (d) Half-reduction times of HyPer, HyPer-2, HyPer-3, and HyPer-H34Y-A406V upon the addition of $H_2O_2$. Zero time corresponds to the maximum of F500/F420 ratio after $H_2O_2$ addition. Error bars indicate standard deviation. Data in panels c and d are results of 7 experiments for HyPer, 10 for HyPer-2, 10 for HyPer-3, and 4 for HyPer-H34Y-A406V; >10 cells in each experiment.

OxyR to bind to a specific region on DNA.[19] In HyPer, these changes alter the fluorescence excitation spectrum thereby shifting the fluorescence intensities after ratiometric excitation at 500 and 420 nm (F500/F420).

Wild-type OxyR functions as a dimer. Its dimerization interface consists of amino acids 226−233 located in the regulatory domain[20] also present in HyPer. On the basis of size-exclusion chromatography data, HyPer is a monomer or weak dimer depending on its concentration.[15] However, it turned out that mutations in the dimerization interface may be critical for the dynamic range of the probe. Mutation A406V in HyPer (corresponding to A233V in OxyR) produced HyPer-2, an indicator with twice expanded dynamic range (maximal change in the F500/F420 ratio upon oxidation) compared to HyPer. HyPer-2 forms a strong dimer showing relatively slow oxidation−reduction kinetics, which can limit temporal resolution of the readout.[15] A233V is a phenotypic mutation in the wtOxyR, which affects the oligomerization state of OxyR structure due to localization in the dimeric interface of the molecule. We proposed that other mutations in the same interface within HyPer or HyPer-2 might lead to a probe with improved oxidation−reduction characteristics, such as higher


dx.doi.org/10.1021/cb300625g | ACS Chem. Biol. 2013, 8, 535−542

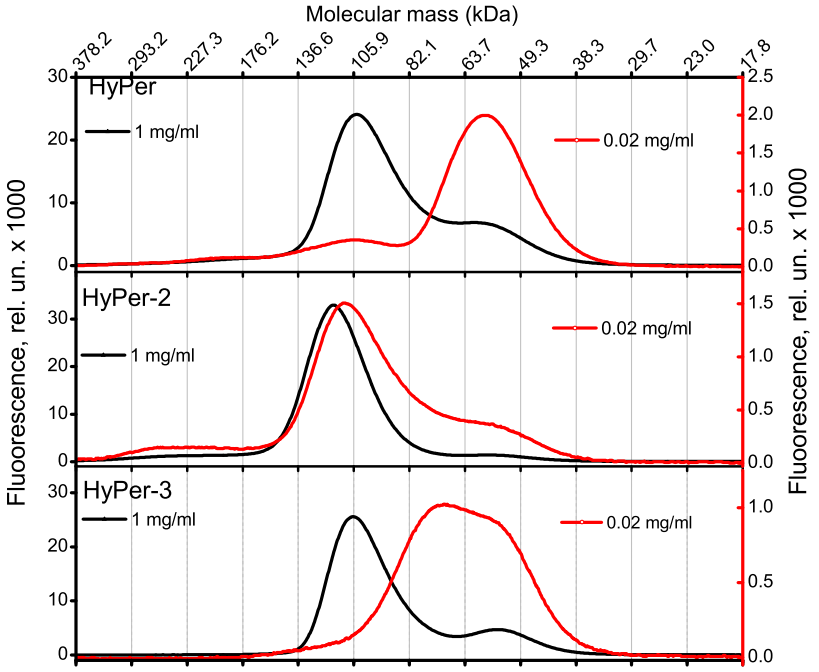


**Figure 2.** Oligomeric state of HyPer-3 versus HyPer and HyPer-2. Gel filtration elution profiles of HyPer, HyPer-2, and HyPer-3.

dynamic range or faster response. Several phenotypic mutations in the OxyR dimerization interface are described in the literature: I110D (constitutively active OxyR), F219A (impaired oxyS induction), L124D (impaired oxyS induction), and H114Y (constitutively active OxyR).[19−21] Although we could not predict how each particular mutation would alter HyPer properties (e.g., A406V enhances dimerization of HyPer, while A233V weakens dimerization of OxyR), we reproduced these mutations in HyPer. While I110D, F219A, and L124D mutations produced variants with extremely low dynamic range, H114Y (corresponds to H34Y in HyPer) substitution resulted in a sensor with high signal-to-noise ratio (Figure 1a,b). We measured oxidation and reduction half-times of HyPer, HyPer-2, and HyPerH34Y. Oxidation half-time of HyPerH34Y (further called HyPer-3) was 1.4-fold faster than the oxidation of HyPer-2. The reduction half-time of HyPer-3 was the shortest of all probes (Figure 1b−d).

Differences in oxidation half-time could stem from different affinities of the probes to $H_2O_2$ or different reaction rates with $H_2O_2$. Since we were not able to isolate the reduced form of HyPer-3, we performed the kinetics measurements using fast fluorescent microscopy of mammalian cells expressing different versions of the probe. Culturing the cells on $\mu$-slides[15] allowed changing $H_2O_2$ concentration in the cells rapidly enough to measure the rate of the pseudofirst order reaction. Minimal concentrations of $H_2O_2$ that were able to induce detectable changes in HyPer fluorescence were 25 nM for the isolated probe and 5−25 $\mu$M for HyPer in *E.coli* or eukaryotic cytoplasm.[14] These data are consistent with data obtained for wtOxyR.[22] Therefore, we estimate a ∼200−500-fold gradient of $H_2O_2$ across the plasma membrane. We determined the concentration of $H_2O_2$ at the half-maximal ($K_{ox}$) reaction rate between the probe and $H_2O_2$ for HyPer to be 160 nM, for HyPer-2 290 nM, for HyPer-3 260 nM (given the 500-fold drop in $[H_2O_2]$ across the plasma membrane). The pseudofirst order reaction rate constants (Ks) were $5 \times 10^5$ $M^{-1}$ $sec^{-1}$ for HyPer, $1.2 \times 10^5$ $M^{-1}$ $sec^{-1}$ for HyPer-2, and $2.5 \times 10^5$ $M^{-1}$ $sec^{-1}$ for HyPer-3. Therefore, the slow response of HyPer-2 originates from a lower, compared to the other probes, reaction rate with $H_2O_2$. HyPer-3 has intermediate values between HyPer and HyPer-2 in both half-oxidation time and reaction rate with $H_2O_2$. Although, it is hard to reconstitute the reduction of HyPer by glutaredoxin or thioredoxin *in vitro*, the differences in half-reduction time of the probes reflect most probably the differences in the reaction rates of the oxidized probes with cellular thiol-reducing systems. The initial decay of the F500/F420 ratio during reduction does not depend too much on residual $[H_2O_2]$ since nearly all molecules of the sensor are oxidized.

In order to compare the brightness of the probes, we isolated them using metal-affinity chromatography. Since we failed to isolate HyPer-3 in its reduced form, the measurements were performed for the oxidized forms of all three probes. All the versions of the sensor had equally low quantum yields of 0.1 but differed in their extinction coefficient (EC). EC/brightness at 490 nm were 17 000/1700, 25 000/2500, and 17 000/1700 $M^{-1}$ $cm^{-1}$ for HyPer, HyPer-2, and HyPer-3, respectively, corresponding to 5−7% of EGFP brightness.

Next, we verified if the combination of the two mutations, A406V and H34Y, could further improve the dynamic range or otherwise affect the sensor properties. HyPer-H34Y-A406V showed the same dynamic range as its parental HyPer-2 and HyPer-3 probes but demonstrated extremely slow half-reduction and half-oxidation times (Figure 1d). Therefore, HyPer-H34Y-A406V cannot be used as a real-time $H_2O_2$ sensor but could be of some potential interest as a memory $H_2O_2$ indicator with the oxidized form lasting for an extended period of time helping to retrospectively identify those cells *in vitro* or *in vivo* that responded to some stimulus by elevating $H_2O_2$.

Mutation H34Y affected the dimerization interface of the OxyR-RD.[21] While HyPer is predominantly monomeric, HyPer-2 forms a strong dimer.[15] Potentially, dimerization is a prerequisite for HyPer dynamic range enhancement. To evaluate the dimerization state of HyPer-3, we performed


dx.doi.org/10.1021/cb300625g | *ACS Chem. Biol.* 2013, 8, 535−542

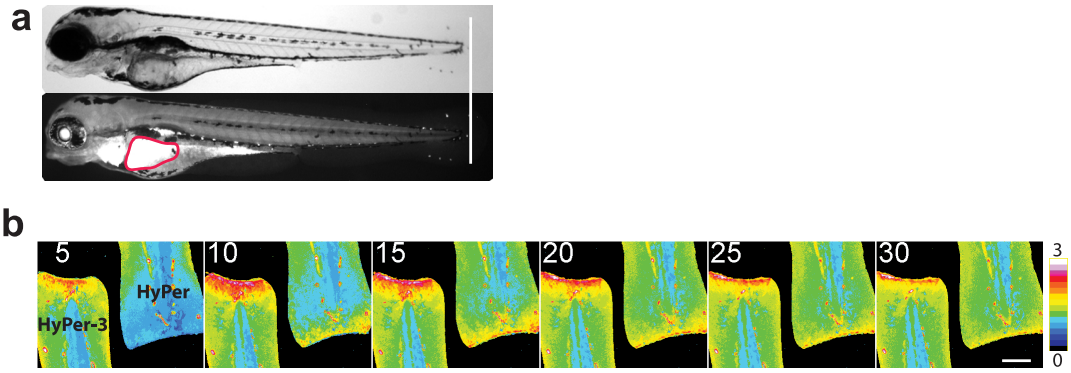


**Figure 3.** HyPer-3 vs HyPer response to wound margin $H_2O_2$ production. (a) Brightfield (upper) and fluorescent (lower) images of $\beta$-actin:HyPer-3 transgenic zebrafish at 3.5 dpf stage. White vertical line indicates the cut plane. Note that the saturated fluorescence in the heart is due to the HyPer-3 construct containing the cmlc2:egfp transgenesis marker (red highlighting) that does not contribute to the fluorescence outside of the heart. (b) Images of F500/F420 ratio in wounded zebrafish embryos expressing HyPer-3 (left embryo) or HyPer (right embryo). Numbers indicate timing in minutes after wounding. Scale bar, 100 $\mu$m. Lookup table indicates F500/F420 ratio.

size-exclusion chromatography. HyPer-3 eluted as a monomer at the 0.02 mg $mL^{-1}$ concentration and as a mixture of monomers and dimers indicating the weak dimeric state of the probe (Figure 2). The strength of dimerization increases in line with HyPer < HyPer-3 < HyPer-2, but this does not directly correlate with the dynamic range since HyPer-2 and HyPer-3 are equal in this respect. Therefore, the dimeric state is not necessary for an increased dynamic range of the probe. However, dimerization seems to affect reaction rates of the oxidized sensors with cellular thiol-reducing machinery since the monomeric versions, HyPer and HyPer-3, are faster in reduction than the strongly dimeric HyPer-2.

Recently, HyPer was successfully used in imaging tissue-scale gradients of $H_2O_2$ upon wounding a zebrafish (*Danio rerio*) at the tail.[23] The gradient started forming within 3 min after wounding and peaked at ~20 min, extending 100−200 $\mu$m into the tail-fin epithelium with a decreasing concentration gradient. The gradient acted to recruit neutrophils to the inflammation site. We tested HyPer-3 performance in this model. We injected mRNA encoding HyPer-3 into the embryo at the stage of a single cell and monitored fluorescence at 3 days postfertilization (dpf). Despite equal brightness of HyPer-3 and HyPer, we were able to detect only weak fluorescence of HyPer-3 *in vivo*. We therefore decided to generate a transgenic zebrafish line expressing HyPer-3 under the ß-actin promoter in order to achieve suitable expression levels. Cells from these transgenic animals exhibited a ubiquitous expression of HyPer-3 (Figure 3a). A transgenic founder with medium strength expression levels was selected for further experiments. Wounding of HyPer-3 expressing animals by cutting the tail fins (Figure 3a) resulted in the appearance of a strong gradient of $H_2O_2$ through the fish tail regions (Figure 3b). Notably, the improved dynamic range of HyPer-3 resulted in higher F500/F420 ratio changes compared to HyPer (Figure 3b). While the maximal change in the ratio was 1.72 ± 0.18 for HyPer, HyPer-3 demonstrated 2.53 ± 0.39-fold ratio elevation (10 HyPer and 7 HyPer-3 embryos from 3 experiments;, data represent mean and SD values). Therefore, HyPer-3 appears to be advantageous for monitoring $H_2O_2$ gradients in tissue. Although HyPer-3 shares the same chromophore and therefore has the same pH-sensitivity as HyPer,[14] previous observations showed that the changes in HyPer ratio upon tail wounding are not caused by pH variations.[23]

Fluorescence lifetime imaging microscopy (FLIM) is an advanced mode of imaging often applied for monitoring biological processes with FRET-based tools.[24,25] Upon changes in the FRET efficiency, lifetimes of the donor fluorophore are altered enabling robust quantification of the relative proportion of molecules in different FRET states. FLIM provides advantages such as the use of a single excitation band for a single probe, quantitative readout, less interference from light scattering or partial photobleaching, and independence of expression level, (wavelength-dependent) reabsorption, or inner filtering. However, the use of FLIM for single-fluorophore based sensors is limited to a few reports of pH-driven lifetime changes in GFP-like proteins.[26] We investigated whether HyPer and HyPer-3 changed fluorescence lifetime upon reaction with $H_2O_2$. We performed frequency-domain FLIM of HyPer and HyPer-3 expressed in HeLa cells before and after adding a saturating amount of $H_2O_2$ (100 $\mu$M). For both probes, the fluorescence intensity of the deprotonated chromophore excited at 488 nm increased and the lifetime decreased upon $H_2O_2$ addition. The data for HyPer-3 are presented in Figure 4a.

For HyPer, the phase and modulation lifetimes were 1.27 ± 0.04 and 1.73 ± 0.02 ns, respectively ($n$ = 20, the number of cells from 3 experiments). The difference between phase and modulation lifetime indicated a multiexponential decay. After the addition of $H_2O_2$, the HyPer phase and modulation lifetime decreased to 1.02 ± 0.06 and 1.44 ± 0.13 ns, respectively ($n$ = 20).

For HyPer-3 (Figure 4a), oxidation decreased the phase and modulation lifetime from 1.29 ± 0.04 (phase) and 1.77 ± 0.05 ns (modulation) to 0.92 ± 0.01 (phase) and 1.12 ± 0.02 ns (modulation) ($n$ = 11). Notably, the fluorescence lifetime of the probes decreased upon oxidation, whereas molecular brightness increased. Since the quantum yield value is proportional to the measured fluorescence lifetime, oxidation of HyPer-3 causes a 25−30% decrease in quantum yield. However, the fluorescence intensity increase up to 5-fold upon oxidation indicated an increase in the extinction coefficient. Taken together, both HyPer and HyPer-3 are suitable for FLIM, but HyPer-3 exhibited more pronounced changes in lifetime upon oxidation.

Finally, we tested the possibility to detect inflammation driven $H_2O_2$ production in zebrafish larvae using FLIM of HyPer-3. The wounding protocol was the same as for


dx.doi.org/10.1021/cb300625g | *ACS Chem. Biol.* 2013, 8, 535−542

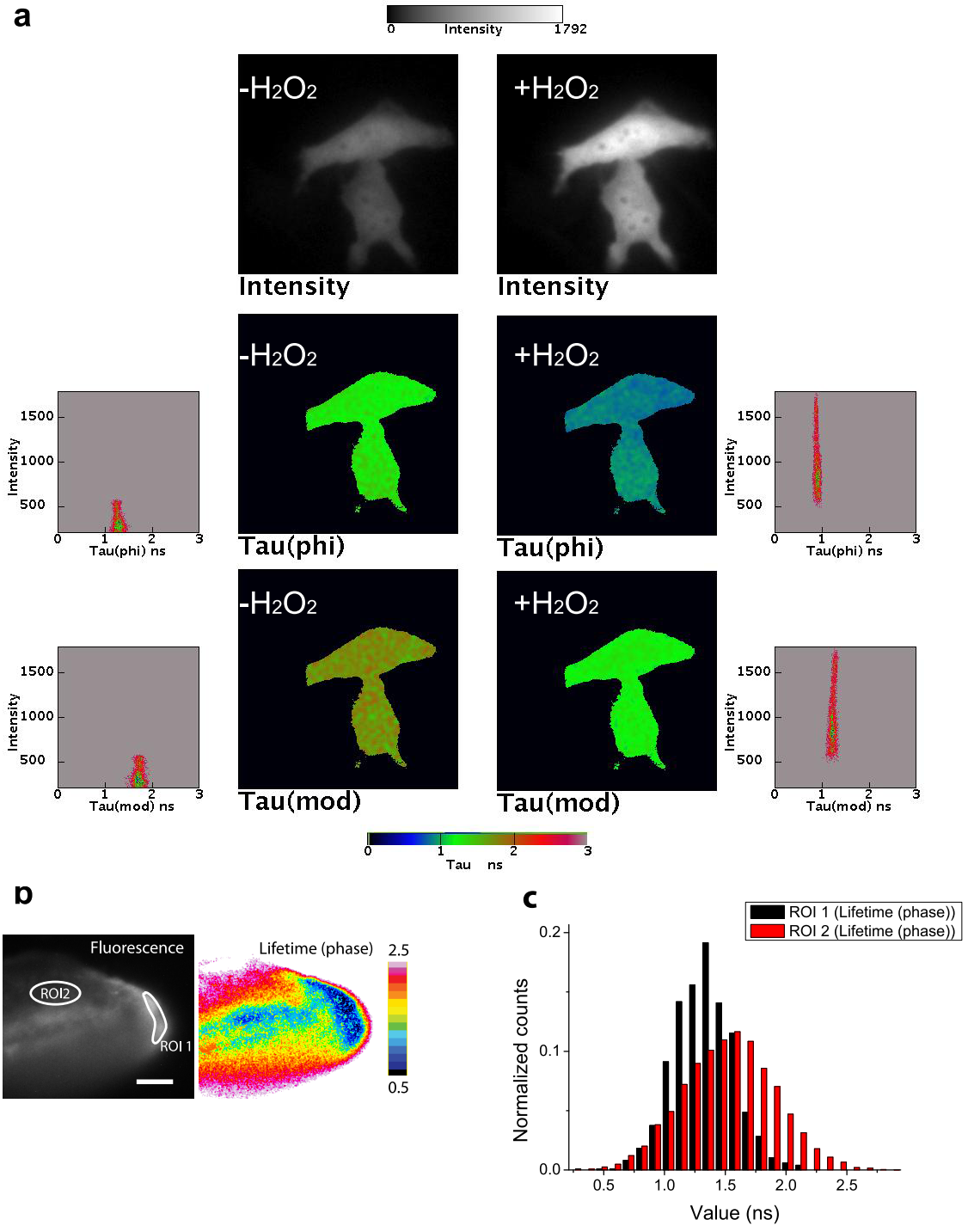


**Figure 4.** Fluorescence lifetime imaging of HyPer-3. (a) FLIM of HyPer-3 response to $H_2O_2$. Left: images obtained in resting HeLa cells expressing HyPer-3. Right: images obtained one minute after adding 100 $\mu$M $H_2O_2$. Images represent from top to bottom the average intensity (note increase upon $H_2O_2$ addition); the phase fluorescence lifetime Tau(phi) with the corresponding dot-plot of fluorescence intensity versus fluorescence lifetime; and the modulation fluorescence lifetime Tau(mod) with the corresponding dot-plot of fluorescence intensity versus fluorescence lifetime. (b) Inflammation driven $H_2O_2$ production in zebrafish larvae imaged using FLIM of HyPer-3. Left and right panels represent fluorescence intensity and FLIM images, respectively. ROI1 highlights the wound margin; ROI2 represents an area distant from the wound. (c) Fluorescence lifetime distribution plot for ROI1 and ROI2 in panel b.

ratiometric imaging described above. We detected lifetime changes in injured animals (Figure 4b). The pattern of the fluorescence lifetime changes was the same for both FLIM (Figure 4b) and ratio (Figure 3b) imaging modes showing the gradient of $H_2O_2$ with higher concentrations of the oxidant at the wounding site.

The FLIM sensitivity of HyPer-3 strongly suggests that this imaging modality might also be applicable to other cpFP-based probes, such as many $Ca^{2+}$ probes,[27] Perceval,[28] Peredox,[29] and others. Besides the intriguing FLIM sensitivity, the F500/F420 ratio is the readout of choice for both HyPer and HyPer-3 due to the more profound change in relative peak brightness.


dx.doi.org/10.1021/cb300625g | ACS Chem. Biol. 2013, 8, 535−542

However, in many applications, FLIM mode could be advantageous. Therefore, the identification and further improvement of the FLIM readout is an important direction in developing single-fluorophore probes such as HyPer.

## METHODS

**Generation of New Versions of HyPer.** For structures containing the desired mutations, we performed site-directed mutagenesis by PCR using the overlap extension of PCR products by primers Pr.1−6 and polymerase Tersus. The original version of HyPer was used as template DNA. Fragments containing the desired mutation were combined into a whole construct containing a point substitution H34Y and A406V by overlap extension PCR. Ligation of all constructs was performed in the vector pQe30 or pC1eGFP, previously subjected to the restriction endonuclease sites *Bam*HI, *Hin*dIII, AsuNHI, and *Hin*dIII (SibEnzyme), respectively.

The selection of useful clones expressing the sensor was carried out using a fluorescent binocular microscope Olympus US SZX12. Spectral characteristics of selected clones were evaluated using a fluorescent spectrophotometer Varian Cary Eclipse. To do this, cells that are descendants of a selected clone in the first stage were collected and suspended in 1 mL of PBS buffer in a fluorimeter cuvette. We detected excitation spectra in the range of 400−510 nm (emission 530 nm) before and after the addition of 250 $\mu$M $H_2O_2$ to the cells.

**Cell Culture and Transfection.** HeLa Kyoto cells were cultured in DMEM with 10% FCS (PAA Laboratories) at 37 °C in a 5% $CO_2$ atmosphere. For imaging experiments, cells were seeded into 35 mm glass bottom dishes (MatTek). After 24 h cells were transfected by a mixture of 1 $\mu$g of DNA and 4 $\mu$L of FuGene6 transfection reagent per one dish. After 6−7 h, cell medium was replaced by fresh medium.

For FLIM experiments, cells were seeded into 24 mm glass coverslips (Menzel-Gläser). After 24 h, cells were transfected by a mixture of 0.5 $\mu$g DNA and 1 $\mu$L Lipofectamin2000 transfection reagent per slide.

**Animal Husbandry.** Zebrafish of the AB strain (wild-type) were maintained and raised in our facility under recommended conditions. All embryos were collected by natural spawning, staged according to Kimmel,[30] and raised at 28 °C in E3 medium (5 mM NaCl, 0.17 mM KCl, 0.33 mM $CaCl_2$, 0.33 mM $MgSO_4$, and 0.1% methylene blue, equilibrated to pH 7.0) in Petri dishes, as described.[31] All animals subjected to experimentation were anesthetized in MS-222, tricaine (Sigma). Procedures at Karlsruhe Institute of Technology comply with the guidelines of national and international animal ethics committees.

**Transgenesis.** An expression vector was generated by recombination of a 5′ entry clone (p5E-bactin2), middle entry clone (pME-HyPer-3), and 3′ entry clone (p3E-polyA) into the destination vector pDestTol2CG2 using the Tol2kit multisite gateway construction kit.[32] The middle entry clone was generated by recombination of a PCR fragment containing HyPer-3 cDNA and corresponding recombination sequences (attB1/attB2) into pDONR221 (#12537−023, Multisite Gateway system, Invitrogen). Transgenesis was performed by coinjection of vector DNA (50 ng/$\mu$L) plus *tol2* mRNA (10 ng/$\mu$L).[33] Resulting transgenics exhibited a ubiquitous expression (b-actin promoter) of HyPer-3. A transgenic founder with medium strength expression levels was selected for further experiments.

**Ratiometric Imaging.** To visualize the fluorescence of transfected cells, 24 h after transfection we used a fluorescence microscope (Leica DMI 6000 B) with a HCX P2 ApoLambda blue 63× NA 1.4 oil objective. Microscopy of cells was carried out at 37 °C in Hank's Balanced Salt Solution supplemented with 20 mM of HEPES. Fluorescence detection was carried out in two channels corresponding to two peaks in the excitation of the cpYFP chromophore (420 and 500 nm) with emission at 510 nm. For the channel corresponding to the protonated form of the cpYFP chromophore (420 nm), we used the following filters: EFW excitation, 427/10 (CFP); emission, BP 542/27 (YFP). For the deprotonated form of the cpYFP chromophore (500 nm). we used the following filters: excitation, BP 504/12 (YFP); emission, BP 542/27 (YFP). Recording intervals were 5 s. To determine the response of the sensor to $H_2O_2$, we added a solution of $H_2O_2$ in 100 $\mu$L volume to the cells to give a final concentration of 150 $\mu$M in the dish.

The final processing of images was performed using the ImageJ software.

**Fluorescence Lifetime Imaging Microscopy.** Frequency-domain FLIM measurements were performed using the setup described earlier.[34] The objective used was a Zeiss Plan Apochromat 63×/1.4 oil-immersion objective. Samples were excited by means of a 488 nm Ar laser modulated at 75.1 MHz and a BP 515/30 nm (Chroma) emission filter was used to detect Hyper fluorescence. FLIM stacks of 12 phase images permutated in recording order[35] were acquired with an exposure time of about 0.1−0.5 s each. $H_2O_2$ was added to the medium at a final concentration of 100 $\mu$M . Image processing was performed with Image J.

FLIM of HyPer-3 expressing zebrafish was performed using LIFA FLIM setup (Lambert instruments) on an Olympus 71 inverted microscope equipped with an Olympus 30× NA 1.05 lens. Excitation was 488 nm, emission in the GFP range. Reference was Atto488.

**Protein Expression and Purification.** Competent *E.coli* XL1Blue cells were transformed with pQE30 plasmid harboring HyPer variant gene. Single colonies were selected on ampicillin, picked, and used to inoculate 200 mL of LB/ampicillin medium (0.5 mg $mL^{-1}$). Bacterial cultures were shaken at 190 rpm for 36−38 h at 37 °C. Bacteria were harvested by centrifugation at 4000*g* for 30 min (4 °C). The pellet was resuspended in 7 mL of buffer A (40 mM Tris-HCl, pH 7.5, containing 150 mM KCl, 10 mM $MgSO_4$, and 5 mM 2-mercaptoethanol), lysed by ultrasound on blue ice bath for 30 min, and clarified by centrifugation at 18 000*g* at 4 °C for 30 min. Proteins were purified from the cell-free extracts by metal-affinity chromatography (Talon Metal Affinity Resin, Clontech). Three milliliters of the cell-free extract was applied to a column filled with resin (column volume, 3.5 mL) equilibrated with buffer A. The column was washed with 35 mL of buffer A (10 volumes), and then, the protein was eluted with 40 mM Tris-HCl, containing 150 mM KCl, 10 mM $MgSO_4$, and 400 mM imidazole. The resulting eluate was immediately applied to a 5 mL Sephadex G-5 column (GE Healthcare) equilibrated with buffer A to remove imidazole.

**Oligomerisation State Estimation.** To determine the oligomeric state of the sensor proteins, we used gel-filtration chromatography performed on a 10/300 GL column with Superdex 200 (Amersham Bioscience) and equilibrated with 40 mM Tris-HCl buffer (pH 7.5). The elution buffer contained 150 mM NaCl. The rate of elution was 0.4 mL/min. We monitored the elution profile by absorbance at 280, 420, and 497 nm using a Varian ProStar 335 detector and by fluorescence using a Varian ProStar 363 fluorescence detector. The molecular masses were calculated from the calibration graph using the known molecular masses of the following proteins: ferritin (440 kDa), catalase (232 kDa), aldolase (158 kDa), BSA (67 kDa), ovalbumin (43 kDa), chymotrypsinogen A (25 kDa), and ribonuclease A (13.7 kDa).

**Spectroscopic Characterization of the Probes.** As we were not able to isolate HyPer-3 in its reduced form, the molar extinction coefficient ($\varepsilon$) and the quantum yield (QY) were measured for the probes in the oxidized form. Equal aliquots of HyPer variants were diluted in PBS, and their absorption spectra were measured in the range 200−600 nm to determine molar extinction coefficients of proteins. The molar extinction coefficients were determined using the formula $\varepsilon_i = \mathrm{Abs}_i \cdot C_{prot}(\mathrm{M})^{-1} \cdot l(\mathrm{cm})^{-1}$, where $\mathrm{Abs}_i$ is the optical density at the absorption maximum, and $l$ is the optical path length.

To determine the quantum yield of fluorescence of HyPer variants, the emission spectra of the fluorescence excited at 485 nm were measured and compared to the protein with known QY (EGFP). QY for each protein was determined using the formula $QY = QY_{EGFP} \cdot Abs1 \cdot Em2 \cdot Abs2^{-1} \cdot Em1^{-1}$, where Abs1 and Em1 are the values of the absorption (485 nm) and emission (510 nm) of EGFP, Abs2 and Em2 are the values of the absorption (485 nm) and emission (520 nm) for HyPer variant, $QY_{EGFP}$ is the quantum yield of fluorescence of EGFP (0,6), and QY is the quantum yield of fluorescence of HyPer variants.

**Sensitivity and Reaction Rates of the Probes.** The half-oxidation constant ($K_{ox}$) and the rate constants ($K_s$) of the reaction


dx.doi.org/10.1021/cb300625g | ACS Chem. Biol. 2013, 8, 535−542

with $H_2O_2$ were determined using fast imaging in the living cells. HeLa-Kyoto cells were cultured on $\mu$-slides-VI (IBIDI) as described before.[15] Cells were transfected and imaged at high speed. $H_2O_2$ was added at final concentrations ranging from 6 to 400 $\mu$M (final concentration) to the separate tracks of $\mu$-slides. The reaction rate ($V$) was determined as $\Delta$ratio/$\Delta$time at the linear region of the curve. $K_{ox}$ was the concentration of $H_2O_2$ at which the reaction rate between HyPer and $H_2O_2$ was the half of the maximum. The pseudofirst order reaction rate constants between HyPer variants and $H_2O_2$ were determined as $K_s = V/[H_2O_2]$.[36]

## AUTHOR INFORMATION


### Corresponding Author

*E-mail: vsevolod.belousov@gmail.com.


### Notes

The authors declare no competing financial interest.

## ACKNOWLEDGMENTS

We thank Olympus for continuous support of the EMBL Advanced Light Microscopy Facility and Y. Belyaev (ALMF, EMBL) for help with imaging and image analysis. This work was supported by the Russian foundation for basic research (RFBR) (10-04-01561-a to V.V.B; 11-04-12187-ofi to S.L), a joint EMBL-RFBR grant (12-04-92427 to C.S. and V.V.B), Measures to Attract Leading Scientists to Russian Educational Institutions program (11.G34.31.0017 to S.L), and the ESF EuroMembrane consortium TraPPs (to C.S. and T.W.J.G.)

## REFERENCES


(1) Droge, W. (2002) Free radicals in the physiological control of cell function. *Physiol. Rev. 82*, 47−95.

(2) Storz, G., and Imlay, J. A. (1999) Oxidative stress. *Curr. Opin. Microbiol. 2*, 188−194.

(3) Segal, A. W., and Jones, O. T. (1978) Novel cytochrome b system in phagocytic vacuoles of human granulocytes. *Nature 276*, 515−517.

(4) Suh, Y. A., Arnold, R. S., Lassegue, B., Shi, J., Xu, X., Sorescu, D., Chung, A. B., Griendling, K. K., and Lambeth, J. D. (1999) Cell transformation by the superoxide-generating oxidase Mox1. *Nature 401*, 79−82.

(5) Bedard, K., and Krause, K. H. (2007) The NOX family of ROS-generating NADPH oxidases: physiology and pathophysiology. *Physiol. Rev. 87*, 245−313.

(6) Winterbourn, C. C. (2008) Reconciling the chemistry and biology of reactive oxygen species. *Nat. Chem. Biol. 4*, 278−286.

(7) D'Autreaux, B., and Toledano, M. B. (2007) ROS as signalling molecules: mechanisms that generate specificity in ROS homeostasis. *Nat. Rev. Mol. Cell Biol. 8*, 813−824.

(8) Denu, J. M., and Tanner, K. G. (1998) Specific and reversible inactivation of protein tyrosine phosphatases by hydrogen peroxide: evidence for a sulfenic acid intermediate and implications for redox regulation. *Biochemistry 37*, 5633−5642.

(9) Lee, S. R., Kwon, K. S., Kim, S. R., and Rhee, S. G. (1998) Reversible inactivation of protein-tyrosine phosphatase 1B in A431 cells stimulated with epidermal growth factor. *J. Biol. Chem. 273*, 15366−15372.

(10) Fomenko, D. E., Xing, W., Adair, B. M., Thomas, D. J., and Gladyshev, V. N. (2007) High-throughput identification of catalytic redox-active cysteine residues. *Science 315*, 387−389.

(11) Weerapana, E., Wang, C., Simon, G. M., Richter, F., Khare, S., Dillon, M. B., Bachovchin, D. A., Mowen, K., Baker, D., and Cravatt, B. F. (2010) Quantitative reactivity profiling predicts functional cysteines in proteomes. *Nature 468*, 790−795.

(12) Miller, E. W., Tulyathan, O., Isacoff, E. Y., and Chang, C. J. (2007) Molecular imaging of hydrogen peroxide produced for cell signaling. *Nat. Chem. Biol. 3*, 263−267.

(13) Meyer, A. J., and Dick, T. P. (2010) Fluorescent protein-based redox probes. *Antioxid Redox Signaling 13*, 621−650.

(14) Belousov, V. V., Fradkov, A. F., Lukyanov, K. A., Staroverov, D. B., Shakhbazov, K. S., Terskikh, A. V., and Lukyanov, S. (2006) Genetically encoded fluorescent indicator for intracellular hydrogen peroxide. *Nat. Methods 3*, 281−286.

(15) Markvicheva, K. N., Bilan, D. S., Mishina, N. M., Gorokhovatsky, A. Y., Vinokurov, L. M., Lukyanov, S., and Belousov, V. V. (2011) A genetically encoded sensor for $H_2O_2$ with expanded dynamic range. *Bioorg. Med. Chem. 19*, 1079−1084.

(16) Gutscher, M., Sobotta, M. C., Wabnitz, G. H., Ballikaya, S., Meyer, A. J., Samstag, Y., and Dick, T. P. (2009) Proximity-based protein thiol oxidation by $H_2O_2$-scavenging peroxidases. *J. Biol. Chem. 284*, 31532−31540.

(17) Kim, S. O., Merchant, K., Nudelman, R., Beyer, W. F., Jr., Keng, T., DeAngelo, J., Hausladen, A., and Stamler, J. S. (2002) OxyR: a molecular code for redox-related signaling. *Cell 109*, 383−396.

(18) Zheng, M., Aslund, F., and Storz, G. (1998) Activation of the OxyR transcription factor by reversible disulfide bond formation. *Science 279*, 1718−1721.

(19) Choi, H., Kim, S., Mukhopadhyay, P., Cho, S., Woo, J., Storz, G., and Ryu, S. (2001) Structural basis of the redox switch in the OxyR transcription factor. *Cell 105*, 103−113.

(20) Kullik, I., Stevens, J., Toledano, M. B., and Storz, G. (1995) Mutational analysis of the redox-sensitive transcriptional regulator OxyR: regions important for DNA binding and multimerization. *J. Bacteriol. 177*, 1285−1291.

(21) Kullik, I., Toledano, M. B., Tartaglia, L. A., and Storz, G. (1995) Mutational analysis of the redox-sensitive transcriptional regulator OxyR: regions important for oxidation and transcriptional activation. *J. Bacteriol. 177*, 1275−1284.

(22) Aslund, F., Zheng, M., Beckwith, J., and Storz, G. (1999) Regulation of the OxyR transcription factor by hydrogen peroxide and the cellular thiol-disulfide status. *Proc. Natl. Acad. Sci. U.S.A. 96*, 6161−6165.

(23) Niethammer, P., Grabher, C., Look, A. T., and Mitchison, T. J. (2009) A tissue-scale gradient of hydrogen peroxide mediates rapid wound detection in zebrafish. *Nature 459*, 996−999.

(24) Bastiaens, P. I., and Squire, A. (1999) Fluorescence lifetime imaging microscopy: spatial resolution of biochemical processes in the cell. *Trends Cell Biol. 9*, 48−52.

(25) van Munster, E. B., and Gadella, T. W. (2005) Fluorescence lifetime imaging microscopy (FLIM). *Adv. Biochem. Eng. Biotechnol. 95*, 143−175.

(26) Nakabayashi, T., Wang, H. P., Kinjo, M., and Ohta, N. (2008) Application of fluorescence lifetime imaging of enhanced green fluorescent protein to intracellular pH measurements. *Photochem. Photobiol. Sci. 7*, 668−670.

(27) Zhao, Y., Araki, S., Wu, J., Teramoto, T., Chang, Y. F., Nakano, M., Abdelfattah, A. S., Fujiwara, M., Ishihara, T., Nagai, T., and Campbell, R. E. (2011) An expanded palette of genetically encoded $Ca^{2+}$ indicators. *Science 333*, 1888−1891.

(28) Berg, J., Hung, Y. P., and Yellen, G. (2009) A genetically encoded fluorescent reporter of ATP:ADP ratio. *Nat. Methods 6*, 161−166.

(29) Hung, Y. P., Albeck, J. G., Tantama, M., and Yellen, G. (2011) Imaging cytosolic NADH−$NAD^+$ redox state with a genetically encoded fluorescent biosensor. *Cell Metab. 14*, 545−554.

(30) Kimmel, C. B., Ballard, W. W., Kimmel, S. R., Ullmann, B., and Schilling, T. F. (1995) Stages of embryonic development of the zebrafish. *Dev. Dyn. 203*, 253−310.

(31) Haffter, P., Granato, M., Brand, M., Mullins, M. C., Hammerschmidt, M., Kane, D. A., Odenthal, J., van Eeden, F. J., Jiang, Y. J., Heisenberg, C. P., Kelsh, R. N., Furutani-Seiki, M., Vogelsang, E., Beuchle, D., Schach, U., Fabian, C., and Nusslein-Volhard, C. (1996) The identification of genes with unique and essential functions in the development of the zebrafish, *Danio rerio*. *Development 123*, 1−36.

(32) Kwan, K. M., Fujimoto, E., Grabher, C., Mangum, B. D., Hardy, M. E., Campbell, D. S., Parant, J. M., Yost, H. J., Kanki, J. P., and Chien, C. B. (2007) The Tol2kit: a multisite gateway-based

construction kit for Tol2 transposon transgenesis constructs. *Dev. Dyn. 236*, 3088−3099.
(33) Urasaki, A., Asakawa, K., and Kawakami, K. (2008) Efficient transposition of the Tol2 transposable element from a single-copy donor in zebrafish. *Proc. Natl. Acad. Sci. U.S.A. 105*, 19827−19832.
(34) Van Munster, E. B., and Gadella, T. W., Jr. (2004) phiFLIM: a new method to avoid aliasing in frequency-domain fluorescence lifetime imaging microscopy. *J. Microsc. 213*, 29−38.
(35) van Munster, E. B., and Gadella, T. W., Jr. (2004) Suppression of photobleaching-induced artifacts in frequency-domain FLIM by permutation of the recording order. *Cytometry, Part A 58*, 185−194.
(36) Dixon, M., Webb, E. C., Thorne, C. J. R., and Tipton, K. F. (1979) *Enzymes*, 3rd ed., Academic Press, New York .